Mixed ionic-electronic conductance across naphthalenediimide-functionalized biopolymer

Ambili Ramanthrikkovil Variyam,[a] Yuval Agam,[a] Alessandro Paradisi,[b] Carlo Augusto Bortolotti,[b] and Nadav Amdursky[a,*]

[a]Schulich Faculty of Chemistry, Technion – Israel Institute of Technology, Haifa 3200003, Israel.

[b]Department of Life Sciences, University of Modena and Reggio Emilia, 41125 Modena, Italy.

*Corresponding author: amdursky@technion.ac.il

Keywords: mixed conductors, biopolymers, conductive polymers, naphthalenediimide, impedance

Abstract

Mixed ionic-electronic conductive polymers are gaining high momentum for several electronic and bioelectronic applications. These polymers are composed of a synthetic conjugated polymer for electronic conduction and a synthetic ionomer for the ionic one. Due to environmental considerations, much effort is being utilized in replacing synthetic polymers with biopolymers. However, to date, the only strategy for making mixed conductors with biopolymers is to blend them with synthetic polymers. Here, we show that by targeting certain amino acids of protein-based biopolymers, we can post-polymerization modify them with naphthalenediimide (NDI), resulting in an improved electronic transport, which is in addition to the native ionic transport of the biopolymers. We further show that by reducing the NDI moieties we can reach conductivity values in the order of 40 $mS \cdot cm^{-1}$, though the NDI can re-oxidize depending on the environment of the biopolymer. The abundant nature of the protein building blocks together with the easy post-polymerization functionalization chemistry of the NDI, which is very much different than any previous use of NDI in conductive polymers, is making our new strategy for making mixed ionic-electronic conductive biopolymers highly attractive.

Introduction

The field of bioelectronics, and specifically, the utilization of organic conductive polymers for the electrical interfacing with biological niches, a sub-field that is usually referred to as organic bioelectronics, has emerged in recent two decades.[1-5] Out of the many conductive polymers that have been explored, we can consider PEDOT:PSS (Poly(3,4-ethylenedioxythiophene)-poly(styrenesulfonate)) as the champion polymer being used in most of the state-of-the-art bioelectronic devices. PEDOT:PSS is a mixed conductor, meaning it can support both electronic transport due to the polymerized conjugated backbone of PEDOT as well as ionic transport due to the sulfonated PSS ionomer. Nevertheless, PEDOT:PSS is a synthetic polymer, and in recent years much work is being employed to replace synthetic polymers with more environmentally friendly alternatives utilizing biological materials for the formation of biopolymers. To date, mostly polysaccharides and proteins are being used for making large-scale free-standing biopolymers from renewable sources,[6] and in this work context, capable to mediate charges. Due to the relatively high water content within biopolymers, and the abundance of side groups capable of participating in a hydrogen bond network, the formed biopolymers are good candidates for ionic transport but not for electronic transport.[7] Some studies have blended conductive polymers into biopolymers to enable electronic transport across them,[8, 9] but this approach is still relying on having a synthetic polymer in the material.

While considering biological systems, electron transport (ET) is mediated by proteins from the nm-scale (such as in the photosystem or our aerobic respiration system)[10] all the way to the macroscale via bacterial nanowires.[11, 12] In all cases, small molecular cofactors, situated within the proteins, are the electron mediators. Using this inspiration, two main approaches have been used to acknowledge ET to macroscopic protein-based biopolymers. The first approach is by genetic manipulation and fusing ET protein containing the cofactor to a structural forming protein[13, 14] or genetically decorating the protein with aromatic amino acids[15, 16] or gold nanoparticles.[17] The second (much simpler) approach is by non-covalent attaching electron mediating cofactors to the protein composing the biopolymer, in a process referred to as molecular doping. In this way, we have previously used protein-based biopolymers that were formed by electrospinning the bovine serum albumin (BSA), and upon relying on the

extraordinary ability of the BSA protein to bind a variety of small molecules, we molecularly doped them with the natural electron mediators of heme.[18, 19] However, even at the maximum doping density of the BSA mat,[20] we could only reach conductivity values in the order of ~3 $mS \cdot cm^{-1}$, which can be considered too low as an electronic conductor, whereas conductive polymers exhibit conductivity of at least dozens of $mS \cdot cm^{-1}$.

Here, we introduce a new strategy for enhancing the electronic transport across the electrospun BSA biopolymers using a post-polymerization modification (PPM). Inspired by the role of π-conjugated molecules in common synthetic conductive polymers,[2] we decided to use a conjugated molecule for the chemical functionalization, for which we chose the naphthalenediimide (NDI) molecule for the PPM. NDI is considered a promising n-type semiconductor owing to its high electron affinity, good carrier mobility, and excellent thermal and oxidative stability.[21] To date, NDI was used for making conductive polymers only by functionalizing it with other moieties, and usually thiophene-based moieties, to increase conductivity.[22-26] In the context of biomaterials, NDI was used to functionalize amphiphile peptides (pre-polymerization) to assist the self-assembly process.[27] Here, we show for the first time the PPM of a biopolymer, the BSA fibers within the mat, with native NDI monomers. Importantly, we show that by reducing the NDI monomers and because of their oriented assembly within the mat, we can reach conductivity values of ~40 $mS \cdot cm^{-1}$. Notably, before the PPM of the BSA mat with NDI, the mat is capable of transporting ions, and specifically protons, along its fibrillar structure.[28, 29] Hence, our new NDI-functionalized BSA mat is considered a mixed ionic-electronic conductor. While the aim of this study is on the novel PPM process of biopolymers with NDI that results in improved electronic processes, we foresee that such biopolymers are good candidates for tissue engineering of electroactive tissues, as shown for instance with synthetic polymers that were functionalized with conjugated oligomers.[30] With that said, due to the physical nature of the BSA mat, being a free-standing fibrous mat with high water content, the use of the BSA mat in ‘traditional’ bioelectronic devices for biosensing applications in the form of thin film field effect transistors is not very viable.

Results and Discussions

NDI monomers were functionalized with the electrospun BSA biopolymer by a two-step process (**Figure 1**). The first step concerns the making of the NDI monomer to be functionalized into the BSA mat. In accordance with previous studies for making NDI monomers,[31, 32] this step involves the imidization of 1,4,5,8–naphthalenetetracarboxylic dianhydride and ethylenediamine. Importantly, the ^{1}H-NMR (**Figure S1**), ^{13}C-NMR (**Figure S2**), and mass spectrum (**Figure S3**) confirm the formation of the monomers and that no polymerization of the monomers took place in this step. The next step was to attach the NDI monomers to the BSA mat using EDC-NHS (1-Ethyl-3-(3-dimethylaminopropyl)carbodiimide-N-hydroxysuccinimide) coupling to carboxylated amino acids (Asp and Glu) within the mat. Following the formation of the NDI-functionalized BSA mat, a clear color change of the mat was observed from a white mat to an orange one (**Figure 1**). The NDI-functionalized BSA mat was characterized by FTIR (**Figure S4** and text within).

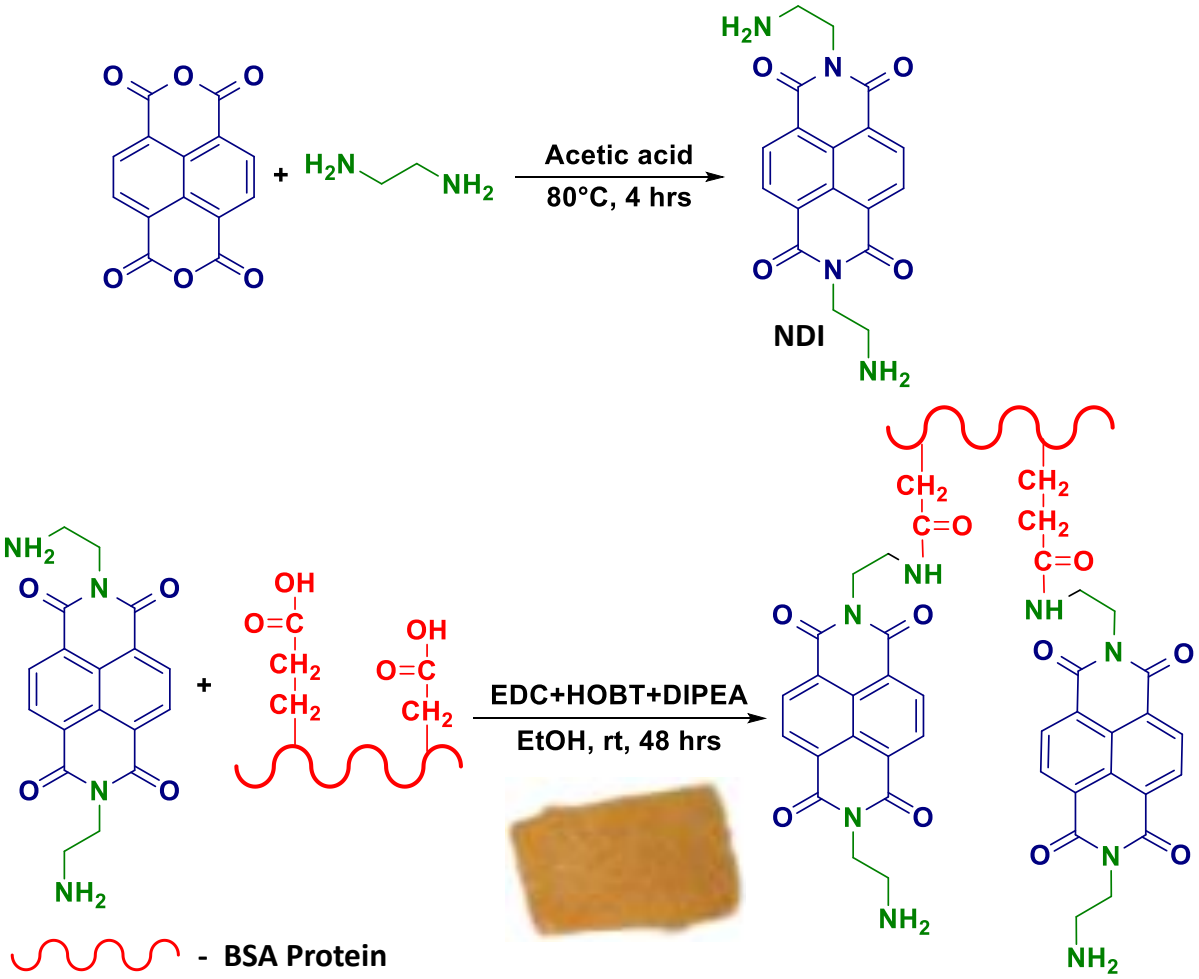

Figure 1. A schematic for the synthesis of the NDI-functionalized BSA mat, together with a picture of the NDI-functionalized BSA mat (a 2×1 cm piece).

Next, we turned to scanning electron microscopy (SEM) measurements for observing the change in the microstructure of the BSA mat upon NDI functionalization. Our SEM images (**Figures 2a-2c**) indicate the formation of an aggregated structure of NDI molecules along the fibers of the BSA mat following functionalization. This might indicate the presence of an alternate ET pathway across the NDI molecules. It is known that the self-assembly of NDI-based molecules influences its conducting properties, where high conductivity values suggest a face-to-face packing of the NDI molecules and enhanced π-π overlap between the naphthalene cores.[33] In addition, we observed a blue shift in the absorption spectrum of NDI following its functionalization with BSA (**Figure 2d**), which suggests the formation of H-

aggregates[34, 35] (face-to-face arrangement) of the NDI in the functionalized mat. According to our observations, we can hypothesize here that the 1-D self-assembly of the NDI molecules on the surface of the BSA fibers within the electrospun mat will facilitate long-range bulk conductivity of the NDI-functionalized BSA mat, as schematically presented in **Figure 2e**.

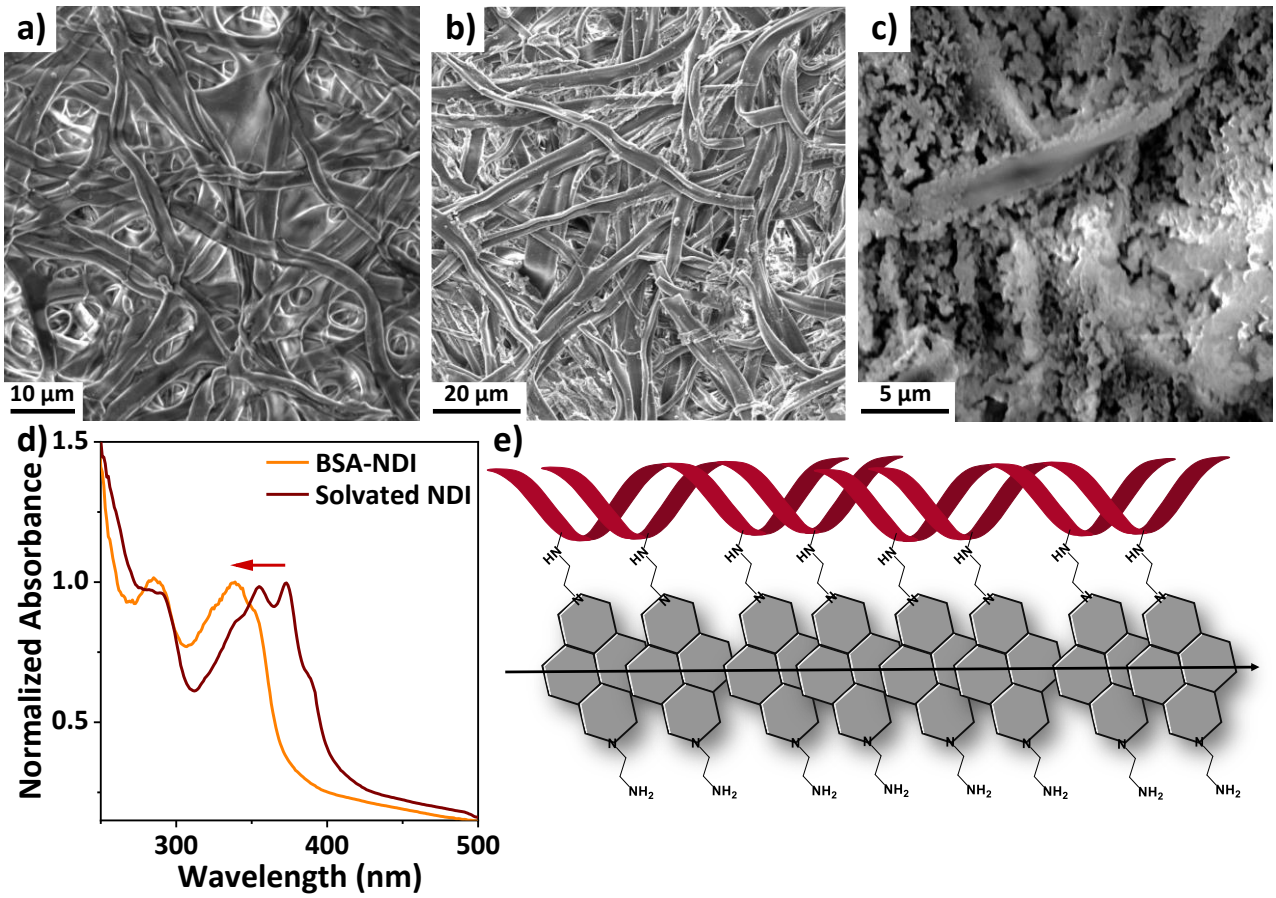

Figure 2. SEM images of (a) the BSA mat and (b) and (c) the NDI-functionalized BSA mat at different magnifications. (d) UV-Vis absorption change between NDI (in EtOH) to the NDI-functionalized BSA mat. (e) An illustration of the suggested hypothesis for the improved electronic conduction across the NDI-functionalized BSA mat.

As stated, the native BSA mat is a proton conductor with a reported conductivity value of ~0.1 $mS \cdot cm^{-1}$.[28, 29, 36] We have used both ac-bias-driven impedance spectroscopy measurements (**Figure 3a**) as well as dc-bias-driven current-voltage (I-V) measurements (**Figure 3b**) to follow the macroscopic conductivity of the NDI-functionalized BSA mat in comparison to the native unfunctionalized mat. As shown in the figures, both for the impedance measurements

(in the form of a Nyquist plot) and the I-V measurements, the NDI-functionalized BSA mat has significantly less resistance than the native BSA mat. It is important here to stress that Figure 3b is showing only the positive bias regime of the I-V response in order to highlight the differences between the BSA before and after the PPM, but since we have a symmetrical electrode configuration also the I-V is symmetric for the negative bias regime (**Figure S5**). For the impedance measurements, we used an equivalent circuit (inset, **Figure 3a**) to fit the results, thus, we can extract the different electronic processes: R1 and R2 being the contact and bulk resistance, respectively, the contact phase element (CPE) is representing the capacitance developed as an electric double layer next to the electrode surface, and the restricted diffusion element (M) is representing a deviation from an ideal Warburg element (the diffusion element). Using R2 and the geometrical dimensions of the specific BSA mat used for each of our repetitions, we calculated a conductivity (σ) value of 4.07±0.22 $mS \cdot cm^{-1}$ for the NDI-functionalized BSA mat compared to ~0.1 $mS \cdot cm^{-1}$ for the native BSA mat, meaning a 40-folds increase in conductivity. In accordance with the dielectric electronic properties of the BSA mat (before or after the PPM), the shape of the I-V is nonlinear, i.e., an increase in the conductance (the derivative of the graph) as a function of bias. Accordingly, we have used the extracted conductance from the low-bias regime of the I-V measurements to compare between the samples, which resulted in a similar level of enhancement for the NDI-functionalized BSA mat as observed with the impedance measurements. We attribute the enhanced conductivity of the NDI-functionalized BSA mat to electronic transport, compared to the sole proton transport in the native BSA mat. Temperature dependence measurements of the impedance spectrum (**Figure 3c**) indicated that the conductance across the NDI-functionalized BSA mat is thermally activated, with calculated activation energy (by fitting to an Arrhenius equation) of 0.26 eV (**Figure 3d**).

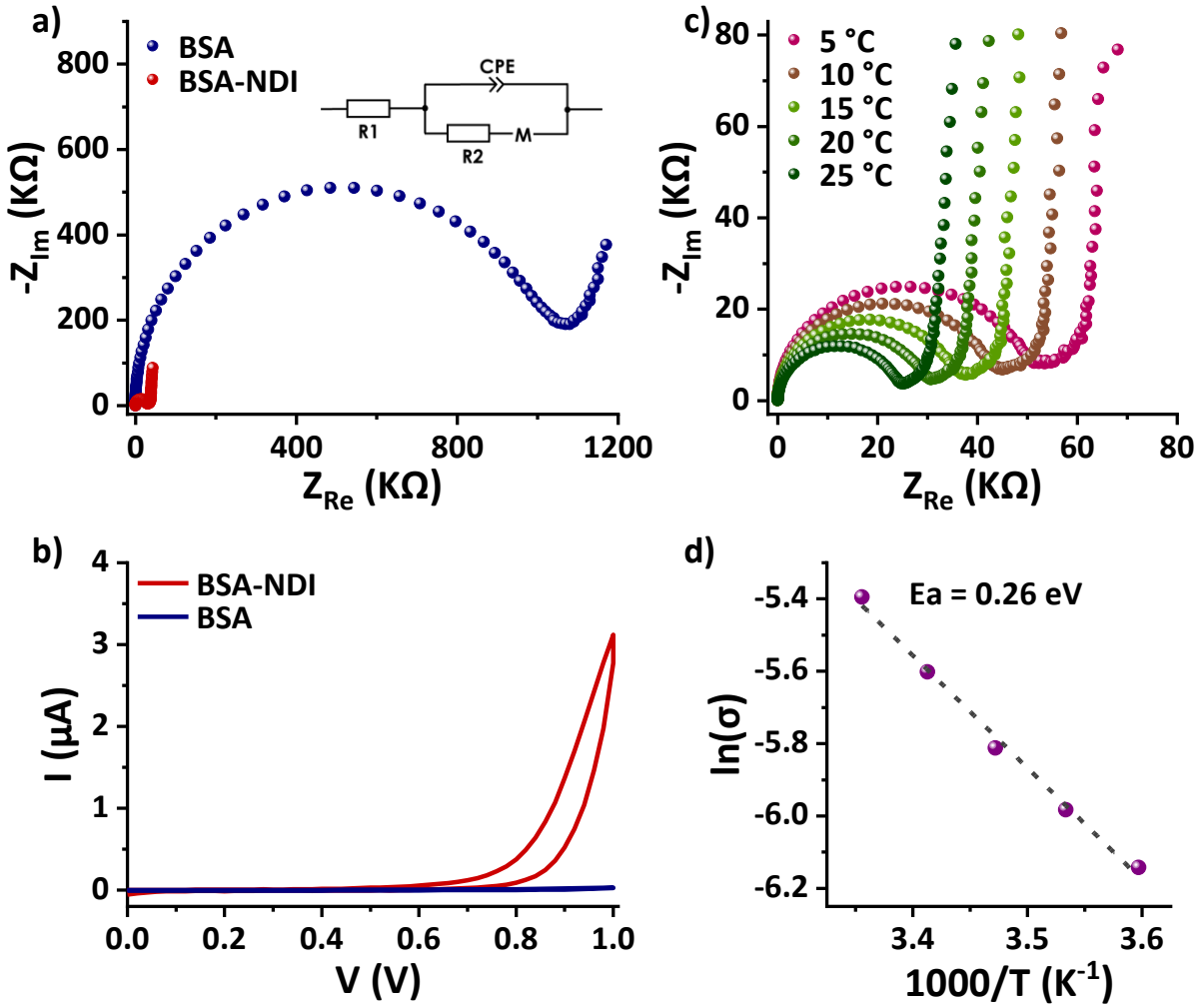

Figure 3. (a) Impedance measurement and (b) I-V measurement comparison between the BSA mat and the NDI-functionalized BSA mat. The inset in (a) shows the equivalent circuit used for fitting the data. (c) Temperature dependency of the measured impedance spectrum for the NDI-functionalized BSA mat, and (d) the extracted activation energy by fitting to an Arrhenius equation. N≥3 for the number of different samples for each measurement.

Until now, we showed that the NDI-functionalized BSA mat exhibited a large increase in conductivity, from 0.1 $mS \cdot cm^{-1}$, which can be ascribed to ionic transport, to a value of 4 $mS \cdot cm^{-1}$ due to the addition of electronic transport. Nonetheless, and as mentioned above, it is still on the lower end compared to many of the common synthetic conductive polymers. As shown for many conductive polymers (e.g., the mentioned PEDOT), electrochemically doping the conjugated moiety can highly influence the ET across it.[37, 38] In a similar manner, the NDI

can be also electrochemically doped to increase the electronic transport across it.[39-43] We implemented this strategy to our NDI-functionalized BSA mat and we reduced the NDI moieties using the common tetra-n-butylammonium fluoride (TBAF) reducing agent,[44-46] by placing the mat following the PPM process in the reducing agent solution (**Figure 4a**). Using UV-Vis spectroscopy, we observed the disappearance of the absorption peak of the NDI monomer at 340 nm and the formation of absorption bands above 400 nm (**Figure 4b**), thus confirming the generation of NDI radical anions following TBAF reduction. We also confirmed by FTIR that the TBAF treatment did not damage the BSA mat itself (**Figure S4** and text within). After reducing with TBAF and washing with acetonitrile the NDI-functionalized BSA mat, we found a further 10-folds increase in conductivity of the reduced NDI-functionalized BSA mat to a value of 39.9±1.9 $mS \cdot cm^{-1}$ (**Figure 4c**), which we ascribed to the formation of free electrons upon reduction. Our control of placing the native BSA mat in the same TBAF solution resulted in no significant change in conductivity (**Figure S6**), thus proving that our observed increase in conductivity is indeed due to reducing NDI, and not related to any change in the BSA mat. The temperature-dependence measurement of the reduced NDI-functionalized BSA mat (**Figure S7a**) showed slightly lower activation energy of 0.2 eV (**Figure S7b**) compared to the NDI-functionalized BSA mat before reduction.

To follow the development of the NDI radical anion as a function of time and concentration of the reducing agent, we designed a series of reduction experiments involving placing the NDI-functionalized BSA mat in varying amounts of TBAF, followed by measuring the conductivity of the now reduced mat at different time points, up to 48 hours in the TBAF solution (**Figure 4d**). As shown in the figure, for all the different concentrations of TBAF, we reached maximum conductivity after around 24 hours of the mat being in the TBAF solution. Furthermore, we see that the more TBAF the higher resulted conductivity up to TBAF concentration of 100 mM in which above this concentration, we did not observe a further increase in the measured conductivity of the reduced NDI-functionalized BSA mat.

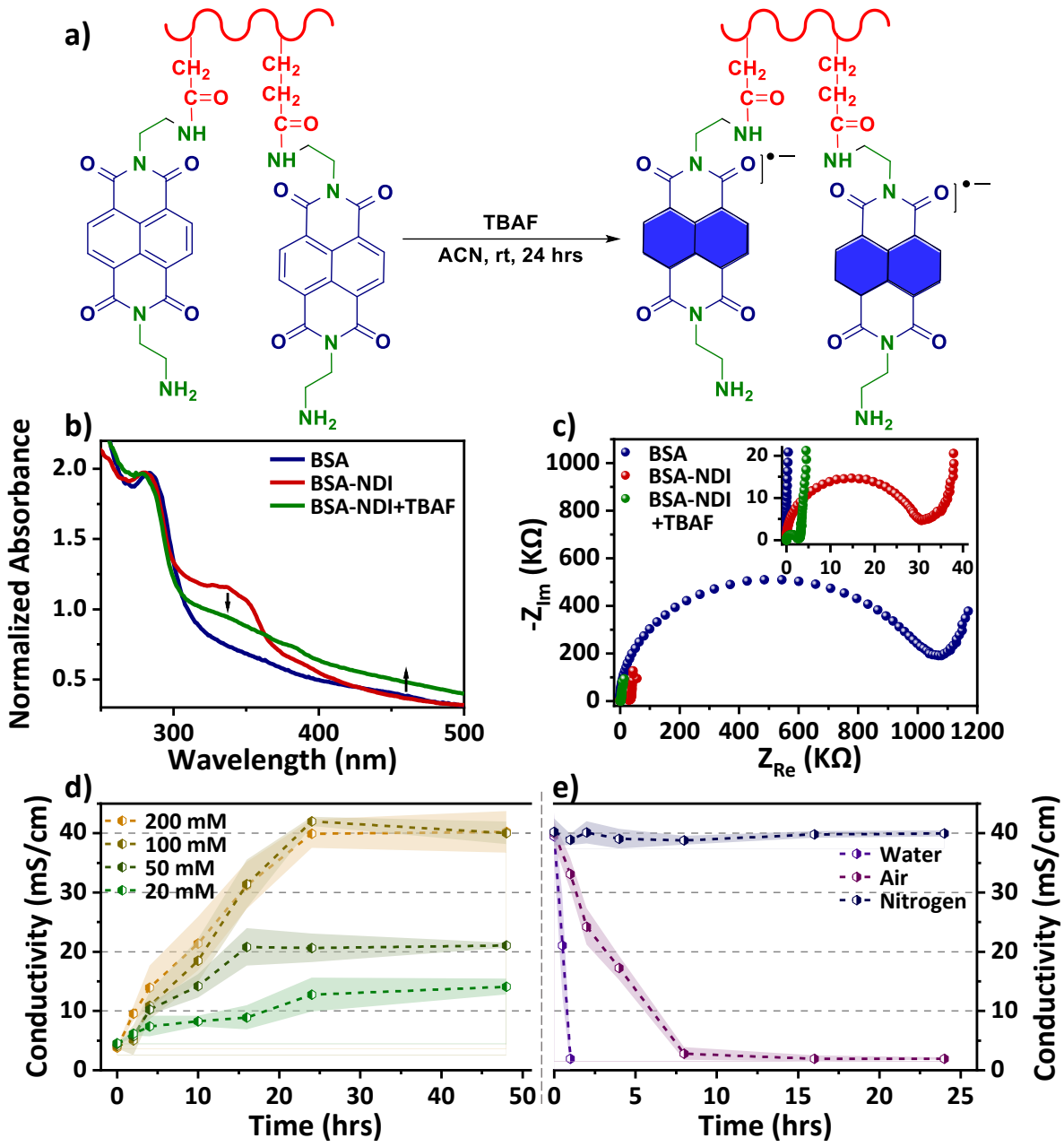

Figure 4. (a) A schematic for the making of the redox NDI-functionalized BSA mat using TBAF. (b) and (c) The change in UV-Vis absorption and measured impedance spectroscopy, respectively, upon reducing the NDI-functionalized BSA mat using TBAF. The inset in (c) is a zoom-in of the low resistance values. (d) and (e) The change in measured conductivity as a function of time for reducing the NDI-functionalized BSA mat using different concentrations of TBAF and the re-oxidation of the reduced NDI-functionalized BSA mat at different environments, respectively (the shaded areas represent the error bars as calculated from the standard deviation of the fitting results). N≥3 for the number of different samples for each measurement.

As common to many conductive polymers, the redox state of the conjugated moiety is highly sensitive to the environment, hence placing the reduced or oxidized conductive polymer in a different environment can lead to the loss of the extra charge, and thus loss of conductivity. To probe the stability of the reduced state of the NDI, we have placed the reduced NDI-functionalized BSA mat in three different environments: inert nitrogen, ambient air, and water, while following the conductivity at different time points (**Figure 4e**). We observed that as long as the NDI-functionalized BSA mat was in inert nitrogen conditions, it did not undergo any loss in its conductivity. However, when the NDI-functionalized BSA mat was placed in ambient conditions, it re-oxidized after around 8 hours. We further found that the redox state of NDI is rapidly changing in water conditions, where we observed the re-oxidation of the material taking place within an hour. Thus, if our strategy here for the formation of mixed conductors will be employed in bioelectronics having an aqueous environment, a different reduction approach should be invoked.

Conclusions

In summary, we have shown here that by a PPM process of a protein-based biopolymer, we can use the NDI monomeric moiety for long-range electronic transport. This is in contrast to all previous reports with the NDI moiety that used an additional synthetic conjugated system for the formation of NDI-based polymers for gaining electronic transport. Moreover, the electronic conductivities of the NDI-functionalized biopolymer, either before the reduction of the NDI (~4 $mS \cdot cm^{-1}$) or after the reduction (~40 $mS \cdot cm^{-1}$), are on the higher end of conductivity values compared to other NDI-based polymers.[42, 43, 47-54] We attribute the high conductivity of the NDI-functionalized BSA biopolymer to our chemical attachment strategy, targeting the many carboxylic acid-containing residues on the surface of the protein composing the biopolymer. As a result, we suggested that the NDI monomers adopt face-to-face packing which promotes efficient electronic transport along the biopolymer. The biopolymer that was used here is based on BSA electrospun mats that have proton conductivity in the order of 0.1 $mS \cdot cm^{-1}$ in their native (unfunctionalized) state, thus the NDI-functionalized BSA mat can be considered as a mixed ionic-electronic conductor. In addition to our strategy here, the use of

free-standing protein-based biopolymers for making mixed conductors is highly novel by itself. Till now, the only strategy of gaining high electronic conductivity for protein-based biopolymers was by blending common synthetic conductive polymer into the biopolymer. Our work here is the first example of a biopolymer showing a mixed conductivity that is solely based on natural proteins and their PPM. Moreover, the abundant and low-cost nature of the BSA proteins and the straightforward and easy chemistry being used for the NDI functionalization during the PPM process is making the NDI-functionalized BSA mat highly attractive by itself. As discussed, we foresee the use of the BSA mat following PPM in regenerative medicine type of applications (or any other application related to the seeding of electroactive cells on a conductive scaffold), and less for biosensing applications that are based on thin films transistor configurations.

Materials and Methods

Electrospinning of BSA mats: Bovine serum albumin (BSA) (MP Biomedicals) was dissolved in 90% 2,2,2-trifluoroethanol (Apollo Scientific) to a final BSA concentration of 14% (weight/volume). After 12 hours, 5% (volume/volume) β-mercaptoethanol (Alfa Aesar) was added into the solution. Electrospinning was performed in a custom-built system with a grounded collector. A 15 kV bias was applied on a 24-gauge blunt needle with an injection rate of 1.5 mL/h. The needle was fixed 12 cm above the collector.

Impedance measurements: Impedance measurements were carried out by using an MTZ-35 impedance/gain-phase analyzer (Bio-Logic). Mats were placed between finger electrodes with an interelectrode distance of 2.5 mm. The finger electrodes were created by evaporating 200 nm Au on top of 40 nm Cr on a glass substrate through a shadow mask using a thermal evaporator at a deposition rate of 2 Å s^{-1} under 5×10^{-7} Torr at room temperature. The finger electrodes were contacted by using a probe station micromanipulator. A 50-mV AC bias was applied during the measurements without applying DC bias. A frequency range of 10 MHz to 10 Hz was used for the experiments. Temperature-dependent studies were performed using a Peltier-containing probe station (INSTEC) in the range of 5°C to 25°C. The conductivity of the

mat was calculated using the following equation: $G = \sigma A/l$, where G is the conductance, σ is the conductivity, A is the cross-sectional area of the mat (A = thickness of mat × width of the mat), and l is the distance between two electrodes. The thickness of the measured BSA mat was ~50 μm and the dimension of the mats was around 1 × 0.5 cm. For each condition, at least three different samples from different batches have been measured for calculating the standard deviation of the fitting results.

Current-voltage measurements: Current-voltage measurements (I-V) were carried out by using an Agilent B2912A Source Meter Unit. Interdigitated Au finger electrodes were patterned onto the SiO_2 substrate *via* photolithography, using a chromium adhesive layer (3–5 nm think). The test pattern was characterized by a channel length (L) of 40 μm and a channel width (W) of 22400 μm (W/L = 560). The BSA mats were placed on top of the interdigitated Au electrodes for the I-V measurements. The current was measured as a function of voltage between 0 V and 1 V, with a scan rate of 100 mV s^{-1}. Similar number of samples have been used in the I-V measurements as mentioned for the impedance measurements.

Spectroscopy and microscopy measurements: NMR measurements were carried out using 400 MHz Bruker Advance III spectrometer. The FTIR spectra were measured using a Bruker Tensor 27 spectrometer equipped with an attenuated total reflectance (ATR). For each measurement, the background was recorded and subtracted from the spectra. The absorption spectra were recorded using a Cary 60 (Agilent) UV–vis spectrophotometer. Morphologies of doped and non-doped BSA mats were characterized using FEI Quanta 200 E-SEM.

Supporting Information

Synthesis and Characterization: NMR, mass spectrum and FTIR; impedance measurement of controls; and temperature-dependent impedance.

Acknowledgments

A.R.V thanks the Sherman fellowship for financial support. N.A. thanks the Binational Science Foundation (grant number 2018239) and the Ministry of Science and Technology (grant numbers 3-16243) for financial support. The present publication has been realized with the joint contribution of the Italian Ministry of Foreign Affairs and International Cooperation (C.A.B) and the Israeli Ministry of Science and Technology (N.A, grant numbers 3-17367). We thank the Russel Berrie Nanotechnology Institute (RBNI) for the support in equipment use.

References

1. M. Berggren and A. Richter-Dahlfors, *Adv. Mater.*, 2007, **19**, 3201-3213.
2. C. Liao, M. Zhang, M. Y. Yao, T. Hua, L. Li and F. Yan, *Adv. Mater.*, 2015, **27**, 7493-7527.
3. J. Rivnay, R. M. Owens and G. G. Malliaras, *Chem. Mater.*, 2013, **26**, 679-685.
4. D. T. Simon, E. O. Gabrielsson, K. Tybrandt and M. Berggren, *Chem. Rev.*, 2016, **116**, 13009-13041.
5. T. Someya, Z. Bao and G. G. Malliaras, *Nature*, 2016, **540**, 379-385.
6. D. L. Kaplan, *Biopolymers from renewable resources*, Springer, 1998.
7. N. Amdursky, E. D. Głowacki and P. Meredith, *Adv. Mater.*, 2019, **31**, 1802221.
8. Y. Wu, Y. X. Chen, J. Yan, D. Quinn, P. Dong, S. W. Sawyer and P. Soman, *Acta Biomater.* , 2016, **33**, 122-130.
9. Y. Xiao, C. M. Li, S. Wang, J. Shi and C. P. Ooi, *J. Biomed. Mater. Res. Part A*, 2010, **92A**, 766-772.
10. H. B. Gray and J. R. Winkler, *Annu. Rev. Biochem.*, 1996, **65**, 537-561.
11. F. Wang, Y. Gu, J. P. O'Brien, S. M. Yi, S. E. Yalcin, V. Srikanth, C. Shen, D. Vu, N. L. Ing, A. I. Hochbaum, E. H. Egelman and N. S. Malvankar, *Cell*, 2019, **177**, 361-369.e310.
12. N. L. Ing, M. Y. El-Naggar and A. I. Hochbaum, *J. Phys. Chem. B*, 2018, **122**, 10403-10423.
13. L. Altamura, C. Horvath, S. Rengaraj, A. Rongier, K. Elouarzaki, C. Gondran, A. L. B. Maçon, C. Vendrely, V. Bouchiat, M. Fontecave, D. Mariolle, P. Rannou, A. Le Goff, N. Duraffourg, M. Holzinger and V. Forge, *Nat. Chem.*, 2017, **9**, 157-163.
14. Y. X. Chen, N. L. Ing, F. Wang, D. Xu, N. B. Sloan, N. T. Lam, D. L. Winter, E. H. Egelman, A. I. Hochbaum, D. S. Clark and D. J. Glover, *ACS Nano*, 2020, **14**, 6559-6569.
15. N.-M. Dorval Courchesne, E. P. DeBenedictis, J. Tresback, J. J. Kim, A. Duraj-Thatte, D. Zanuy, S. Keten and N. S. Joshi, *Nanotechnology*, 2018, **29**, 454002.
16. N. L. Ing, R. K. Spencer, S. H. Luong, H. D. Nguyen and A. I. Hochbaum, *ACS Nano*, 2018, **12**, 2652-2661.
17. D. M. Shapiro, G. Mandava, S. E. Yalcin, P. Arranz-Gibert, P. J. Dahl, C. Shipps, Y. Gu, V. Srikanth, A. I. Salazar-Morales, J. P. O'Brien, K. Vanderschuren, D. Vu, V. S. Batista, N. S. Malvankar and F. J. Isaacs, *Nat. Commun.*, 2022, **13**, 829.
18. N. Amdursky, X. Wang, P. Meredith, D. J. Riley, D. J. Payne, D. D. C. Bradley and M. M. Stevens, *Adv. Mater.*, 2017, **29**, 1700810.

19. C.-C. Hsu, A. Serio, N. Amdursky, C. Besnard and M. M. Stevens, *ACS Appl. Mater. Interfaces*, 2018, **10**, 5305-5317.
20. Y. Agam, R. Nandi, A. Kaushansky, U. Peskin and N. Amdursky, *Proc. Natl. Acad. Sci. U.S.A.*, 2020, **117**, 32260-32266.
21. M. A. Kobaisi, S. V. Bhosale, K. Latham, A. M. Raynor and S. V. Bhosale, *Chem. Rev.*, 2016, **116**, 11685-11796.
22. Z. H. Chen, Y. Zheng, H. Yan and A. Facchetti, *J. Am. Chem. Soc.*, 2009, **131**, 8-9.
23. F. S. Kim, X. G. Guo, M. D. Watson and S. A. Jenekhe, *Adv. Mater.*, 2010, **22**, 478-482.
24. H. Kruger, S. Janietz, D. Sainova, D. Dobreva, N. Koch and A. Vollmer, *Adv. Funct. Mater.*, 2007, **17**, 3715-3723.
25. H. Yan, Z. H. Chen, Y. Zheng, C. Newman, J. R. Quinn, F. Dotz, M. Kastler and A. Facchetti, *Nature*, 2009, **457**, 679-686.
26. X. G. Guo, F. S. Kim, M. J. Seger, S. A. Jenekhe and M. D. Watson, *Chem. Mater.*, 2012, **24**, 1434-1442.
27. N. Singha, P. Gupta, B. Pramanik, S. Ahmed, A. Dasgupta, A. Ukil and D. Das, *Biomacromolecules*, 2017, **18**, 3630-3641.
28. Y. Agam, R. Nandi, T. Bulava and N. Amdursky, *Mater. Adv.*, 2021, **2**, 1739-1746.
29. N. Amdursky, X. Wang, P. Meredith, D. D. C. Bradley and M. M. Stevens, *Adv. Mater.*, 2016, **28**, 2692-2698.
30. K. I. Ritzau-Reid, C. D. Spicer, A. Gelmi, C. L. Grigsby, J. F. Ponder Jr., V. Bemmer, A. Creamer, R. Vilar, A. Serio and M. M. Stevens, *Adv. Funct. Mater.*, 2020, **30**, 2003710.
31. C. T. Miller, R. Weragoda, E. Izbicka and B. L. Iverson, *Bioorganic & Medicinal Chemistry*, 2001, **9**, 2015-2024.
32. M. B. Avinash, E. Verheggen, C. Schmuck and T. Govindaraju, *Angew. Chem. Int. Edit.*, 2012, **51**, 10324-10328.
33. M. Pandeeswar, H. Khare, S. Ramakumar and T. Govindaraju, *Chem. Commun.*, 2015, **51**, 8315-8318.
34. S. Ghosh, X. Q. Li, V. Stepanenko and F. Wurthner, *Chem. Eur. J.*, 2008, **14**, 11343-11357.
35. F. Wurthner, T. E. Kaiser and C. R. Saha-Moller, *Angew. Chem. Int. Ed.*, 2011, **50**, 3376-3410.
36. S. Mondal, Y. Agam, R. Nandi and N. Amdursky, *Chem. Sci.*, 2020, **11**, 3547-3556.
37. J. Ouyang, Q. F. Xu, C. W. Chu, Y. Yang, G. Li and J. Shinar, *Polymer*, 2004, **45**, 8443-8450.
38. I. Lee, G. W. Kim, M. Yang and T. S. Kim, *ACS Appl. Mater. Interfaces*, 2016, **8**, 302-310.
39. S. Wang, H. Sun, T. Erdmann, G. Wang, D. Fazzi, U. Lappan, Y. Puttisong, Z. Chen, M. Berggren, X. Crispin, A. Kiriy, B. Voit, T. J. Marks, S. Fabiano and A. Facchetti, *Adv. Mater.*, 2018, **30**, 1801898.
40. Y. Wang, M. Nakano, T. Michinobu, Y. Kiyota, T. Mori and K. Takimiya, *Macromolecules*, 2017, **50**, 857-864.
41. C. Y. Yang, M. A. Stoeckel, T. P. Ruoko, H. Y. Wu, X. J. Liu, N. B. Kolhe, Z. Wu, Y. Puttisong, C. Musumeci, M. Massetti, H. D. Sun, K. Xu, D. Y. Tu, W. M. Chen, H. Y. Woo, M. Fahlman, S. A. Jenekhe, M. Berggren and S. Fabiano, *Nat. Commun.*, 2021, **12**, 2354.
42. N. Cho, H. L. Yip, J. A. Davies, P. D. Kazarinoff, D. F. Zeigler, M. M. Durban, Y. Segawa, K. M. O'Malley, C. K. Luscombe and A. K. Y. Jen, *Adv. Energy Mater.*, 2011, **1**, 1148-1153.

43. Y. L. Liang, Z. H. Chen, Y. Jing, Y. G. Rong, A. Facchetti and Y. Yao, *J. Am. Chem. Soc.*, 2015, **137**, 4956-4959.
44. Y. Han, Z. P. Fei, Y. H. Lin, J. Martin, F. Tuna, T. D. Anthopoulos and M. Heeney, *npj Flexible Electron.*, 2018, **2**, 11.
45. T. L. D. Tam and J. W. Xu, *Chem. Commun.*, 2019, **55**, 6225-6228.
46. A. F. Paterson, A. Savva, S. Wustoni, L. Tsetseris, B. D. Paulsen, H. Faber, A. H. Emwas, X. X. Chen, G. Nikiforidis, T. C. Hidalgo, M. Moser, I. P. Maria, J. Rivnay, I. McCulloch, T. D. Anthopoulos and S. Inal, *Nat. Commun.*, 2020, **11**, 3004.
47. K. Al Kurdi, S. A. Gregory, S. Jhulki, M. Conte, S. Barlow, S. K. Yee and S. R. Marder, *Mater. Adv.*, 2020, **1**, 1829-1834.
48. D. Nava, Y. Shin, M. Massetti, X. C. Jiao, T. Biskup, M. S. Jagadeesh, A. Calloni, L. Duo, G. Lanzani, C. R. McNeill, M. Sommer and M. Caironi, *ACS Appl. Mater. Interfaces*, 2018, **1**, 4626-4634.
49. S. B. Schmidt, M. Honig, Y. H. Shin, M. Cassinelli, A. Perinot, M. Caironi, X. C. Jiao, C. R. McNeill, D. Fazzi, T. Biskup and M. Sommer, *ACS Appl. Mater. Interfaces*, 2020, **2**, 1954-1963.
50. B. D. Naab, S. Y. Zhang, K. Vandewal, A. Salleo, S. Barlow, S. R. Marder and Z. A. Bao, *Adv. Mater.*, 2014, **26**, 4268-4272.
51. R. A. Schlitz, F. G. Brunetti, A. M. Glaudell, P. L. Miller, M. A. Brady, C. J. Takacs, C. J. Hawker and M. L. Chabinyc, *Adv. Mater.*, 2014, **26**, 2825-2830.
52. A. Higgins, S. K. Mohapatra, S. Barlow, S. R. Marder and A. Kahn, *Appl. Phys. Lett.*, 2015, **106**, 163301.
53. B. D. Naab, X. D. Gu, T. Kurosawa, J. W. F. To, A. Salleo and Z. A. Bao, *Adv. Electron. Mater.*, 2016, **2**, 1600004.
54. Y. Zhang, H. Phan, H. Q. Zhou, X. N. Zhang, J. Y. Zhou, K. Moudgil, S. Barlow, S. R. Marder, A. Facchetti and T. Q. Nguyen, *Adv. Electron. Mater.*, 2017, **3**, 1600546.